



Numerical Simulations of the Slingatron

by Gene R. Cooper, Derek A. Tidman, Mark Bundy,
and Stephen Wilkerson

ARL-RP-30

September 2001

A reprint from Proceedings of the 10th U.S. Army Gun Dynamics Symposium,
Austin, TX, 23-26 April 2001.

20010926 053

Approved for public release; distribution is unlimited.

The findings in this report are not to be construed as an official Department of the Army position unless so designated by other authorized documents.

Citation of manufacturer's or trade names does not constitute an official endorsement or approval of the use thereof.

Destroy this report when it is no longer needed. Do not return it to the originator.

Army Research Laboratory

Aberdeen Proving Ground, MD 21005-5066

ARL-RP-30

September 2001

Numerical Simulations of the Slingatron

Gene R. Cooper, Mark Bundy, and
Stephen Wilkerson

Weapons and Materials Research Directorate, ARL

Derek A. Tidman

ALCorp.

A reprint from Proceedings of the 10th U.S. Army Gun Dynamics Symposium, Austin,
TX, 23-26 April 2001.

Approved for public release; distribution is unlimited.

Abstract

The slingatron mass accelerator is described for several track configurations (shapes), and numerical simulations of this accelerating mass traversing a given track configuration are presented. The sled is modeled as a point mass that interacts with the slingatron track using both a conventional and a new empirical velocity dependent friction law. The closed loop circular slingatron was found to produce high maximum sled velocities provided the gyration angular speed is always increasing. In contrast several spiral shaped slingatron tracks reveal that high maximum sled velocities are obtainable with the gyration speed held constant. In fact, a slingatron constructed out of semi-circles is shown capable of generating high velocity sleds in such a way that no initial sled injection is necessary. Choosing the proper initial gyration phase with an empirically determined friction model allows the mass sled to gain ever-increasing velocities when placed in a semi-circle slingatron. The sled bearing pressure and its total acceleration are examined and presented.

Numerical Simulations of the Slingatron

G. R. Cooper¹, D. A. Tidman^{*}, M. Bundy¹, S. Wilkerson¹

¹U.S. Army Research Laboratory, Aberdeen Proving Ground, Maryland 21005-5066

^{*}ALCorp., 6801 Benjamin Street, McLean, VA 22101

Abstract

The slingatron mass accelerator is described for several track configurations (shapes), and numerical simulations of this accelerating mass traversing a given track configuration are presented. The sled is modeled as a point mass that interacts with the slingatron track using both a conventional and a new empirical velocity dependent friction law. The closed loop circular slingatron was found to produce high maximum sled velocities provided the gyration angular speed is always increasing. In contrast several spiral shaped slingatron tracks reveal that high maximum sled velocities are obtainable with the gyration speed held constant. In fact, a slingatron constructed out of semi-circles is shown capable of generating high velocity sleds in such a way that no initial sled injection is necessary. Choosing the proper initial gyration phase with an empirically determined friction model allows the mass sled to gain ever-increasing velocities when placed in a semi-circle slingatron. The sled bearing pressure and its total acceleration are examined and presented.

Nomenclature

$\mathbf{A} =$	acceleration vector
$A_{//} =$	\mathbf{n} component of \mathbf{A}
$A_{\perp} =$	\mathbf{m} component of \mathbf{A}
$D =$	sled diameter
$\mathbf{F} =$	force vector acting on sled $F = \mathbf{F} $
$F_{//} =$	\mathbf{n} component of \mathbf{F}
$F_{\perp} =$	\mathbf{m} component of \mathbf{F}
$f =$	spin frequency of gyration vector
$\dot{f} =$	time derivative of gyration frequency f
$\mathbf{i}, \mathbf{j}, \mathbf{k} =$	Cartesian unit triad
$L =$	sled length
$M =$	mass of sled
$\mathbf{m} =$	normal unit vector on concave side of track
$\mathbf{n} =$	normal unit vector anti-parallel to the track
$P =$	bearing pressure
$\mathbf{R} =$	sled radius vector $ \mathbf{R} = R$
$\mathbf{r} =$	gyration vector $ \mathbf{r} = r$
$s =$	displacement
$t =$	time

$V =$	velocity $V = \sqrt{\dot{x}^2 + \dot{y}^2}$
$\hat{V} =$	relative sled velocity
$x =$	abscissa of sled
$y =$	ordinate of sled
$\alpha =$	orientation angle $= \phi - 2\pi[(\phi/2\pi)]$
$\delta =$	differences between upper and lower semi-circle radii
$\theta =$	lock-in angle
$\gamma =$	ratio of specific heats
$\lambda =$	radius of curvature
$\mu =$	coefficient of friction
$\rho =$	diameter of circle
$\phi =$	orientation of R
$\psi =$	orientation of r
$\psi_0 =$	initial value of ψ
$ =$	absolute value
$(') =$	$d()/d\phi$
$(\dot{ }) =$	$d()/dt$
$\langle \rangle =$	average value
$\times =$	vector product
$[x] =$	greatest integer $\leq x$

Introduction

A mechanical method for accelerating a mass to high velocities has been proposed by D. A. Tidman² using a device called the slingatron¹. Several closed loop slingatron configurations have previously been examined. For these configurations the accelerated mass (called a sled in this report) interaction with the slingatron track was modeled with magnetic levitation¹ or with a mechanical friction force that is proportional to the normal force exerted by the track² on the sled. This report presents numerical simulations of slingatrons having several different track configurations. The sled and track interaction continues to be treated as a normal force friction model but now the friction coefficient, μ , is either a constant or an empirically determined function depending on the sleds velocity relative to the slingatron track.

These simulations reveal that the mass can be accelerated to very high velocities for each track configuration (track shape) examined here. Generally, the calculations show that spiral shaped slingatrons will produce high velocities for constant gyration speeds and the single loop circular slingatron will produce high velocities for sufficiently high gyration acceleration. We emphasize that the main reason this happens is that the sled locks into a constant phase angle as it transverses the slingatron track. When this occurs the sleds velocity is optimally increased for each 2π revolution of the sled. This will continue until the frictional force dominates the component of the Coriolis force that is parallel to the slingatron track. However, there are cases where parameters can be chosen so the parallel component of the Coriolis force is always greater than the force due to friction. In such cases one will find that the non-relativistic sled velocity increases

indefinitely. In the spiral slingatrons lock-in occurs almost instantaneously while for the single loop circular slingatron lock-in occurs after a sufficient amount of time has passed.

Theory

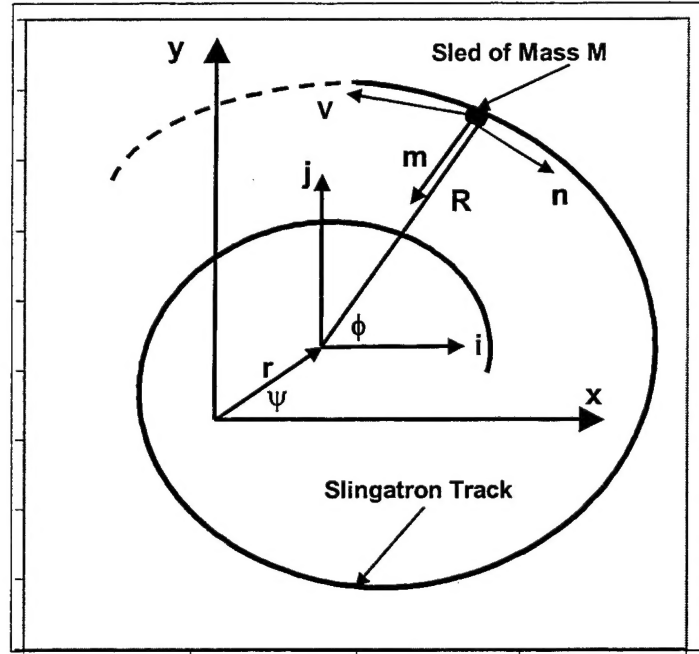


Figure 1 Schematic of a general slingatron

Figure 1 shows a sled of mass M moving along a track with position $\mathbf{R} + \mathbf{r}$ and corresponding velocity $\mathbf{V} = \dot{\mathbf{R}} + \dot{\mathbf{r}}$. The sleds velocity is assumed large enough so that it stays in contact with the track at all times. In fact, the velocity may be large enough to cause mass loss due to abrasion or evaporation, i.e., $\dot{M} \neq 0$. The force \mathbf{F} acting on the sled can be written as $\mathbf{F} = F_{\perp} \mathbf{m} + F_{\parallel} \mathbf{n}$ where \mathbf{m} and \mathbf{n} are unit vectors pointing normal (toward the concave side of the track) and anti-parallel to the track. Therefore, $\mathbf{n} = -\mathbf{R}'/R'$ and $\mathbf{m} = \mathbf{n} \times \mathbf{k}$ for unit vector \mathbf{k} pointing out along the normal to the plane

of the track. Calling the unit vectors along the abscissa and ordinate \mathbf{i} and \mathbf{j} allows the momentum equations, see Fig. 1, to be written as

$$\begin{aligned} (\dot{M}\dot{x} + M\ddot{x}) &= -(\sin(\phi)(F_{\perp}R' - F_{\parallel}R) + \cos(\phi)(F_{\perp}R + F_{\parallel}R'))/\sqrt{R'^2 + R^2} \\ (\dot{M}\dot{y} + M\ddot{y}) &= -(\sin(\phi)(F_{\perp}R + F_{\parallel}R') + \cos(\phi)(F_{\parallel}R - F_{\perp}R'))/\sqrt{R'^2 + R^2} \end{aligned} \quad (1)$$

with Cartesian coordinates (x, y) in the (\mathbf{i}, \mathbf{j}) plane which are constrained so that

$$\begin{aligned} x &= R \cos(\phi) + r \cos(\psi) \\ y &= R \sin(\phi) + r \sin(\psi) \end{aligned} \quad (2)$$

The parallel force F_{\parallel} is assumed to be caused by friction and therefore the standard friction model is represented as

$$F_{\parallel} = \mu(\hat{V})F_{\perp} \ni \hat{V} = |\dot{\phi}|\sqrt{R'^2 + r^2} \quad (3)$$

for which \hat{V} is the sled velocity relative to the track. Now solving Eqs. (1) for F_{\perp} and F_{\parallel} and then including Eq. (2) and Eq. (3) results in the following differential equation

$$\begin{aligned} \ddot{\phi} &= -\frac{\dot{\phi}^2(\mu(R^2 - RR'' + 2R'^2) + R'(R + R''))}{R^2 + R'^2} \\ &+ \frac{((M(\ddot{\psi} + \mu\dot{\psi}^2) + \dot{M}\dot{\psi})\sin(\psi - \phi) + (M\dot{\psi}^2 - \mu(M\ddot{\psi} + \dot{M}\dot{\psi}))\cos(\psi - \phi))rR'}{M(R^2 + R'^2)} \\ &+ \frac{((M(\dot{\psi}^2 - \mu\ddot{\psi}) - \mu\dot{M}\dot{\psi})\sin(\psi - \phi) - (M(\ddot{\psi} + \mu\dot{\psi}^2) + \dot{M}\dot{\psi})\cos(\psi - \phi))rR'}{M(R^2 + R'^2)} \\ &- \frac{\dot{M}\dot{\phi}}{M} \end{aligned} \quad (4)$$

Equation (4) is general enough to account for many slingatron configurations as long as the motion takes place in the \mathbf{i}, \mathbf{j} plane. The configurations are obtained by specifying the ϕ dependence of the vector $\mathbf{R}(\phi)$ giving the shape of the slingatron track. The

friction coefficient, $\mu(\hat{V})$, the time dependent mass, $M(t)$, and the gyration angle, $\psi(t)$, must also be given in order to numerically integrate Eq. (4)

Circular Slingatron

This report considers several possible track configurations all of which treat the length of the gyration arm, $|\mathbf{r}| = r$, as a constant. The first consideration is the circular slingatron^{1,2} defined by

$$|\mathbf{R}(\phi)| = \text{constant} . \quad (5)$$

In general we have found that any slingatron will optimally accelerate a sled to high velocities whenever the lock-in angle, $\theta = \psi - \phi$, is very close to constant i.e.

$$\begin{aligned} \dot{\theta} &\approx 0 \text{ hence} \\ \dot{\psi} &\approx \dot{\phi} \text{ and } \ddot{\psi} \approx \ddot{\phi} \end{aligned} \quad (6)$$

Using the constraints given by Eq. (5) and Eqs. (6) simplifies Eq. (4) to the following expression

$$\begin{aligned} \ddot{\phi} &= b \dot{\phi}^2 \\ b &= \frac{r(\sin(\theta) - \mu \cos(\theta)) - \mu R}{r(\mu \sin(\theta) + \cos(\theta)) + R} \end{aligned} \quad (7)$$

for constant μ and M . This is easily integrated to give us the sleds velocity

$$V = \sqrt{\dot{x}^2 + \dot{y}^2} \text{ as}$$

$$V = \frac{|\dot{\phi}(0)| \sqrt{2rR \cos(\theta) + R^2 + r^2}}{|1 - \dot{\phi}(0) b t|} . \quad (8)$$

A plot of Eq. (8) is shown in Fig. 2 for $\theta = \pi/4$ $\phi(0) = 0$ and $\dot{\phi}(0) = \pi$. One can see that the non-relativistic velocity V becomes infinite at the time $t_{\infty} = 1/\dot{\phi}(0)b$ whenever we force θ to be constant^{1,2}.

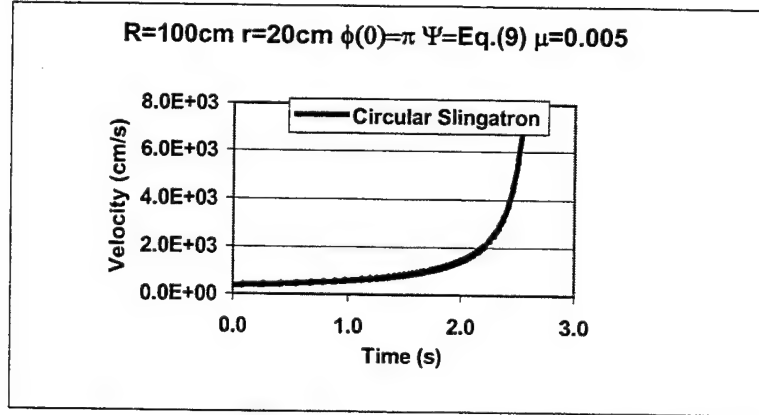


Fig. 2 Velocity vs. time for the circular slingatron

The values of t_{∞} change rapidly in regions where $\theta \approx \pi n$, $n = 0, 1, 2, \dots$ and therefore a plot of $t_{\infty}(\theta)$ is given in Fig. 3.

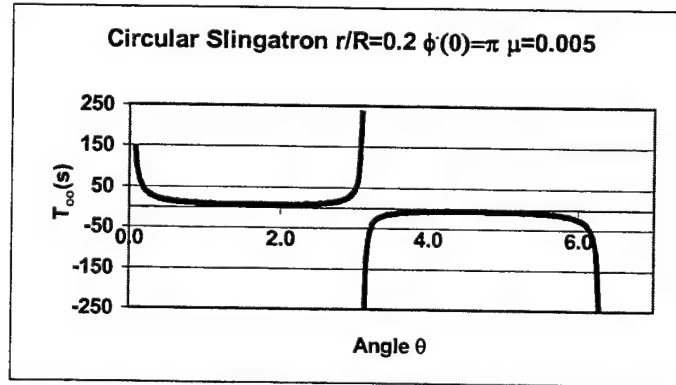


Fig. 3 $t_{\infty}(\theta)$ vs. time for the circular slingatron

Equation (7) shows that $b = 0$ whenever

$$\theta = \pm 2 \tan^{-1} \left(\sqrt{(\alpha^2 - 1)\mu^2 + \alpha^2} \mp \alpha / (\alpha - 1)\mu \right) \pm \pi n, n = 0, 1, 2$$

assuming $(\alpha^2 - 1)\mu^2 + \alpha^2 \geq 0$

(9)

These results used in Eq. (8) produce two time independent velocities given by $V = |\dot{\phi}(0)| \left| \sqrt{(\alpha^2 - 1)\mu^2 + \alpha^2} \mp 1 \right| / \sqrt{\mu^2 + 1}$. A small amount of algebra reveals that constant velocities occur when the normal force becomes so large that friction prevents the sled from accelerating along the circular track. Hence, the sleds velocity stays constant.

Instead of demanding the constraints given by Eqs (6) lets now consider a circular slingatron with an accelerating angular gyration speed such that

$$\psi = \psi_0 + 2\pi f t + \pi \dot{f} t^2.$$
(10)

Numerically integrating Eq. (4), subject to Eq. (10), produces the velocity, with initial conditions $\phi(0) = 0$ and $\dot{\phi}(0) = 2\pi f$, plotted in Fig. 4. Here we see that high velocities are obtained for $\dot{f} \neq 0$.

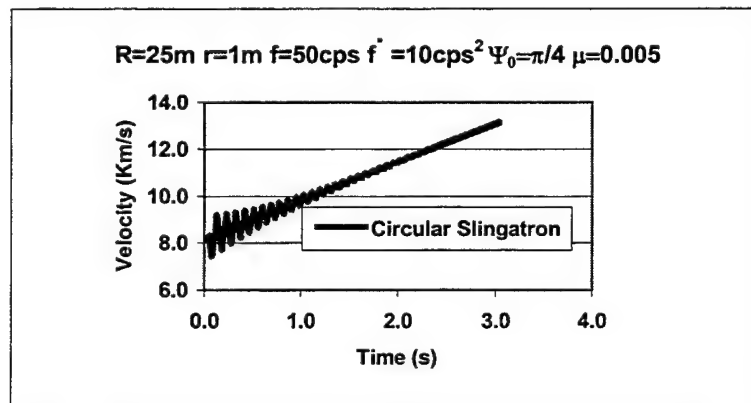


Fig. 4 Velocity vs. time for the driven circular slingatron

The corresponding lock-in angle, $\theta = \psi - \phi$, found in Fig. 5 becomes relatively constant when sled velocities become large.

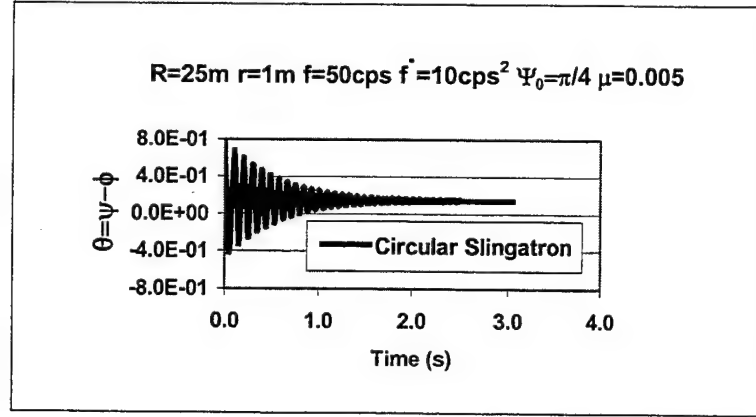


Fig. 5 Lock-in angle vs. time for the driven circular slingatron

Even though high sled velocities can be obtained with a circular slingatron it is encumbered with the difficulty of creating an easy exit port for the high-speed sled. To alleviate this mechanical difficulty we will next examine possible open loop spiral slingatrons.

Archimedes Spiral Slingatron

We now focus our study on configurations that are not closed loop slingatrons. In particular, we examine spiral shaped tracks having open ends, which have the advantage of an easy exit for an accelerated sled entering free flight. Following Tidman² we first examine an Archimedes spiral shaped slingatron track given by

$$R = R_i + r\phi \sin(\psi_0) \quad (11)$$

for which the constant R_i is the initial radius and spacing between adjacent spirals is determined by $\sin(\psi_0)$. The gyration speed is now held constant so that the expression given in Eq. (10) is replaced with

$$\psi = \psi_0 + 2\pi f t. \quad (12)$$

Tidman³ presents a first order analysis for a sled with $\dot{M} = 0$ and μ held constant.

Putting Eq. (11) into Eq. (4) and keeping first order terms, i.e. terms first order in

$O\left(\frac{r}{R}, \dot{\mu}\right)$, leads to the simple equation with $\theta = \psi - \phi$

$$V'/V = (r \sin(\theta))/R(\phi) - \mu. \quad (13)$$

Integrating this result shows that the average increase in velocity, ΔV , for the sled during a 2π revolution of a single spiral leads to the following expression for averaged quantities

$$\Delta V/\text{cycle} \approx 2\pi \langle V \rangle [(r \sin(\theta))/R(\phi) - \mu]. \quad (14)$$

With this motivation we now place Eqs. (10-11) into Eq. (4) and follow with numerical integration to produce the velocity plot, $V(t) = \sqrt{\dot{x}^2 + \dot{y}^2}$, found in Fig. 5. The initial conditions are $\phi(0) = 0$, $\dot{\phi}(0) = 2\pi f$ and the sled mass plus the coefficient μ are both held constant.

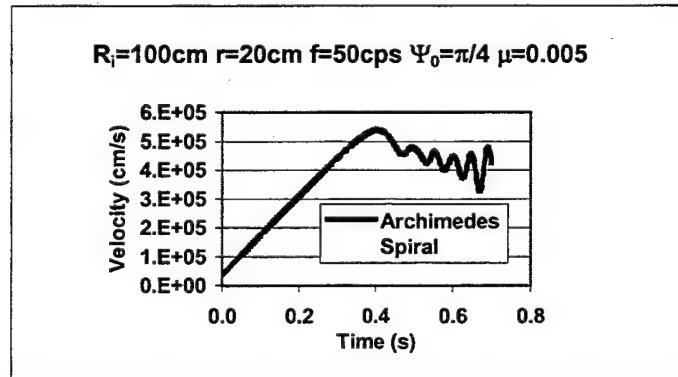


Fig. 6 Velocity vs. time for the Archimedes spiral slingatron

We immediately see that the maximum velocity has the same order of magnitude as that found for the circular slingatron, see Fig. 2, but does so in far less time and requires no acceleration of the gyration arm. The radius $R(\phi)$ changes so that the lock-in angle, θ , stays relatively constant until the sled has reached its maximum velocity as shown in Fig7.

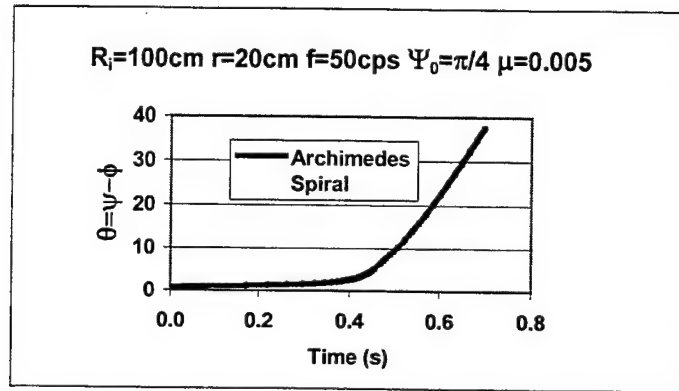


Fig. 7 Lock-in angle vs. time for the Archimedes spiral slingatron

Inspecting Eq. (14) one can infer that the maximum velocity occurs where the frictional force, between the sled and track, balances the parallel component of the Coriolis force as the sled moves along the spiral track. A plot presented in the following section will provide numerical confirmation of this conclusion.

Semi-Circle Slingatron

The next slingatron configuration examined, is constructed using a sequence of semi-circles³ having increasing radii, see Fig. 8.

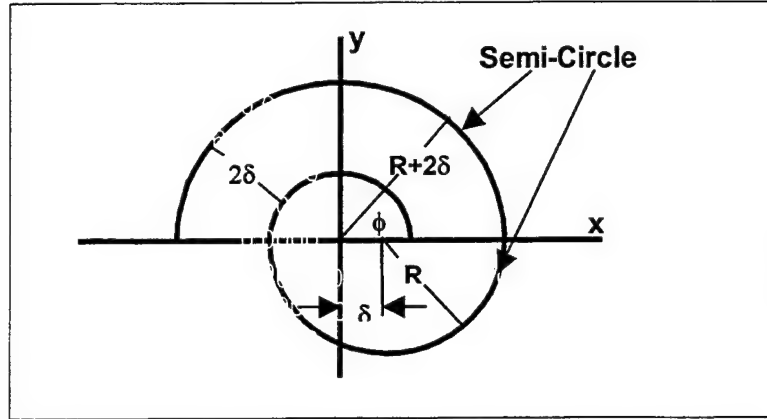


Fig. 8 Schematic of the semi-circle slingatron

We note this slingatron continues to have the sled exit advantage found for the Archimedes slingatron. However, this track has the added advantage in that large sled velocities can be obtained without the need of initial sled injection, i.e. $\phi(0)=0$ and $\dot{\phi}(0)=0$, provided the slingatron has been scaled up to a sufficiently large size. All of the previous slingatrons plus the small-scale high frequency version of the present slingatron require initial sled injection, $\dot{\phi}(0) \neq 0$, in order to obtain large maximum velocities. Because of these advantages a more thorough investigation including sled pressure loads and an empirical friction model, incorporating mass loss $\dot{M} < 0$, is presented. According to Fig. 8 the semi-circles in the upper half plane are described by

$$\begin{aligned}
 R &= R_i + 2\delta \lfloor \phi/2\pi \rfloor \\
 R' &= 0 \\
 R'' &= 0 \\
 \delta &= \pi r \sin(\psi_0)
 \end{aligned}
 \tag{15}$$

and applying the law of cosines to this geometry we find for the semi-circles in the lower half plane having center coordinates at $(\delta, 0)$ are described as

$$\begin{aligned}
R &= \delta \cos(\phi) + \sqrt{(R_i + 2\delta \lfloor \phi/2\pi \rfloor + \delta)^2 - \delta^2 \sin^2(\phi)} \\
R' &= \frac{\delta R \sin(\phi)}{\delta \cos(\phi) - R} \\
R'' &= \frac{R'^2 + 2\delta R' \sin(\phi) + \delta R \cos(\phi)}{\delta \cos(\phi) - R}
\end{aligned} \tag{16}$$

Putting Eq. (15) and Eq. (16) into Eq. (4) followed with numerical integration leads to sled velocities shown in Fig. 9.

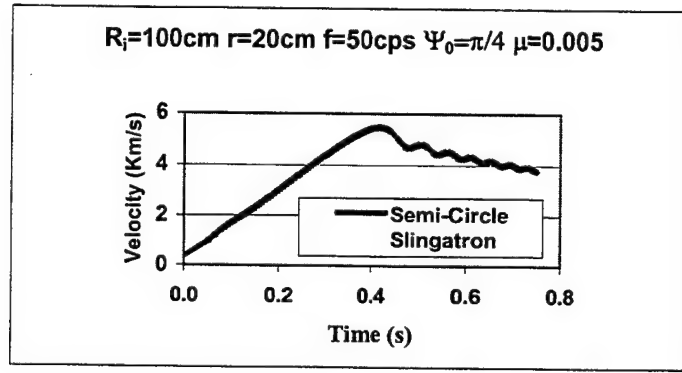


Fig. 9 Velocity vs. time for the semi-circle slingatron

This high frequency small-scale slingatron, i.e. $f = 50\text{cps}$ and $R_i = 100\text{cm}$, is subjected to the conditions $\phi(0)$, $\dot{\phi}(0) = 2\pi f$, $\dot{M} = 0$, and $\mu = 0.005$. Figure 10 tells us again that the lock-in angle θ diverges, from nearly a constant value, after the time, t , where the sled reaches its maximum velocity.

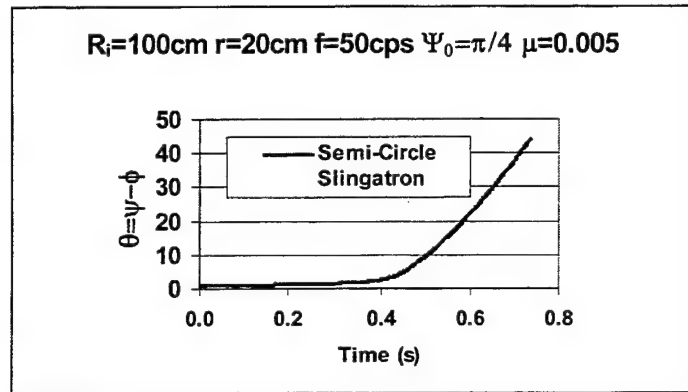


Fig. 10 Lock-in angle for the semi-circle slingatron

An important simplification, when constructing a semi-circle slingatron, occurs when we consider a large-scale version, i.e. $f=11\text{cps}$ and $R_i=400\text{cm}$, of this slingatron. For these cases we can generate large maximum velocities without the need for an initial sled injection velocity. An example of this is depicted in Fig. 11 such that $\phi(0)=0$, $\dot{\phi}(0)=0$ and the sled mass as well as the friction coefficient are still held constant.

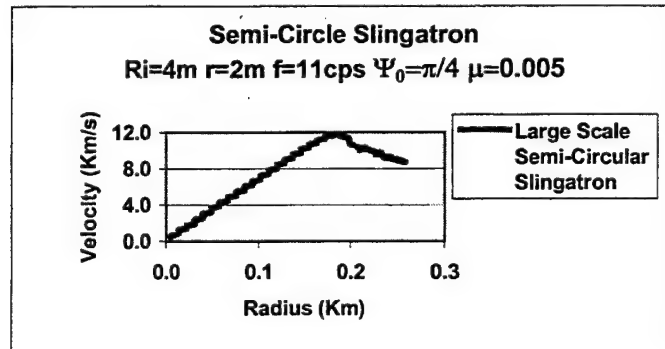


Fig. 11 Velocity vs. radius for the large-scale semi-circle slingatron

This plot has the time axis replaced by radial distance to indicate the size of this large-scale example. In contrast we note that the small-scale version, of this slingatron, still

requires a non-zero initial sled velocity, $\dot{\phi}(0) \neq 0$, in order to obtain a significantly larger maximum sled velocity.

To address a more realistic slingatron one should consider the interaction between the sled and the slingatron track. Therefore, we will assume that the sled is covered with material that abrades, $\dot{M} < 0$, as it moves along the track, in such away that the removed mass acts as a lubricant. As the velocity increases the abraded particles may become a liquid bearing and at still greater velocities the liquid will eventually evolve into a gas or even a plasma. To date only a preliminary experimental investigation of the friction coefficient, $\mu(\hat{V})$, dependence on the sleds relative speed \hat{V} , has been carried out by Tidman³. The preliminary data for a lexan sled indicate that

$$\mu(\hat{V}) = \frac{0.152}{(1 + 3.16\hat{V})} \quad (17)$$

$$\hat{V} = \dot{\phi} \sqrt{R'^2 + R^2}$$

where \hat{V} is measured in Km/s, ranging up to a maximum velocity of 2.0 Km/s. The corresponding value of \dot{M} is still very suspect but the preliminary data gives the following estimation

$$\dot{M} = -\frac{M\hat{V}}{50\pi R(\phi)} \quad (18)$$

Tidman² has suggested that if the velocity, and therefore the bearing pressure between the track and the sled, is large enough to cause the abrading mass to gasify one might then assume

$$\dot{M} = -\frac{\mu M \hat{V}}{\gamma(\gamma-1)R(\phi)} \quad (19)$$

for lexan $\gamma \approx 1.25$

The two estimates found in Eqs. (18-19) are plotted in Fig. 12 while assuming the friction coefficient given by Eq. (17) remains true for all velocities.

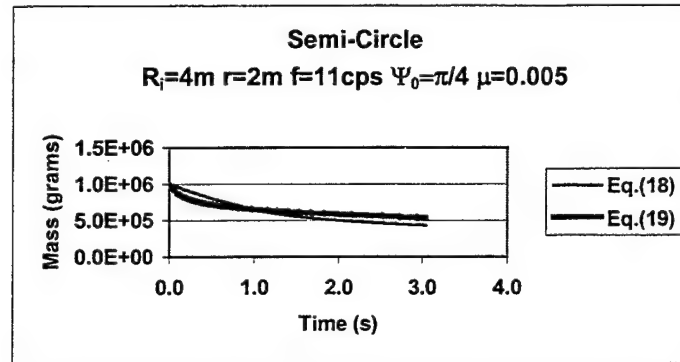


Fig. 12 Sled mass vs. time for the semi-circle slingatron

Figure 13 shows the velocity results for a constant mass sled plus the two cases where $\dot{M} \neq 0$ given by Eqs. (18-19). Since there is no discernable difference between the three cases we will select $\dot{M} = 0$ for the remainder of this paper.

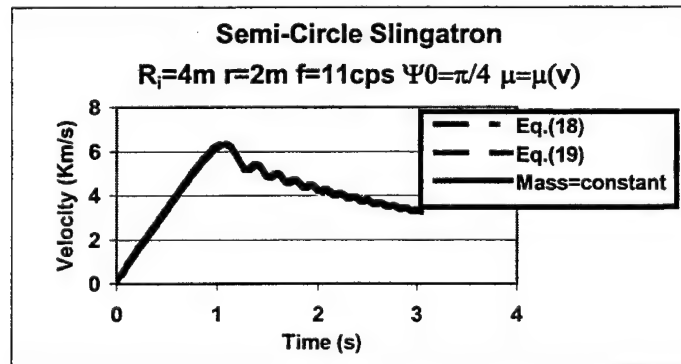


Fig. 13 Velocity comparison vs. time as functions of M and \dot{M}

This selection should not be taken as a general conclusion since the present results stem from two simple \dot{M} models. All that we can claim here is that the dynamics represented by Eq. (4) are weekly dependent on our two \dot{M} models. A more in-depth study of the bearing physics may reveal that \dot{M} cannot be ignored in a more elaborate friction model and therefore \dot{M} must be included in the momentum equations.

To demonstrate the importance of the friction model we next compare our empirical model, Eq. (17), to the constant friction model $\mu = 0.005$. Figure 14 has an example comparison of the sled velocity using initial conditions $\phi(0) = 0$ and $\dot{\phi}(0) = 0$ for these two models.

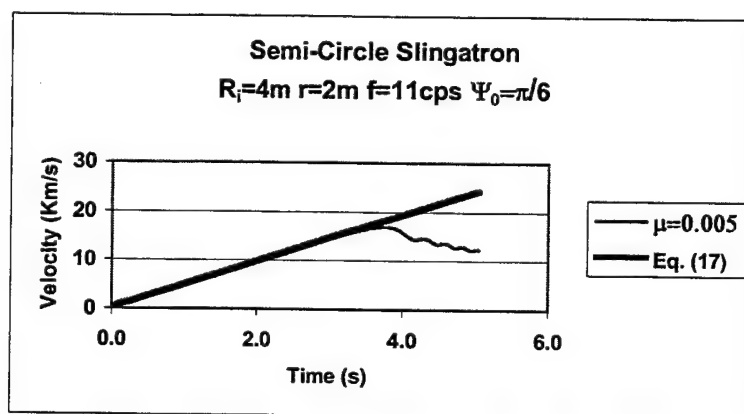


Fig. 14 Velocity comparison vs. time as a function of μ

We see that Eq. (17) and the initial phase $\psi_0 = \pi/6$ can lead to classically unlimited velocities imparted to the sled. This is an example force due to friction never becomes large enough to overcome the parallel component of the Coriolis acceleration.

To gain insight into the magnitudes of the bearing pressure exerted by the sled on a semi-circle slingatron one can examine a typical right cylinder shaped lexan-coated sled

having length L and diameter D . Assuming that the ablating material exerts a uniform pressure along the half lateral surface of the sled facing the slingatron track, one will find the pressure P is easily calculated to be $P = F_{\perp}/DL$. An example of bearing pressure, for a sled with initial mass $M = 1.0 \times 10^3 \text{ Kg}$, plotted as a function of time is presented in Fig. 15.

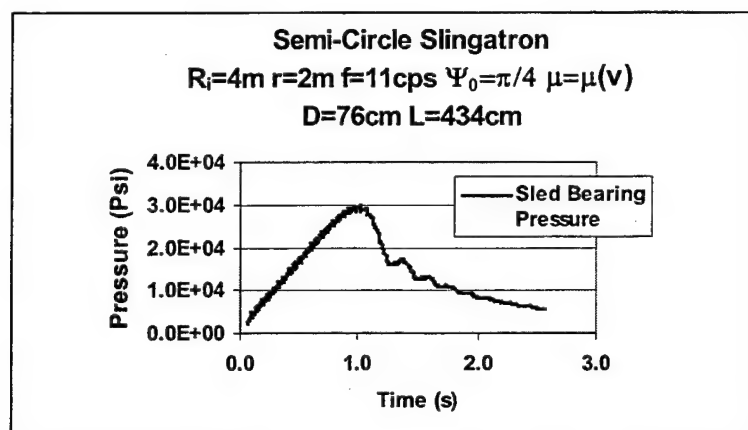


Fig. 15 Sled bearing pressure vs. time for semi-circle slingatron

Calculating the sleds acceleration along the unit vectors \mathbf{m} and $-\mathbf{n}$ while the traversing the slingatron track may also prove useful to the designer. Remembering that the normal component of the acceleration is always pointing toward the concave side of the track we can find its magnitude from $A_{\perp} = V^2/\lambda$. An example, for the large-scale slingatron, is shown in Fig. 16.

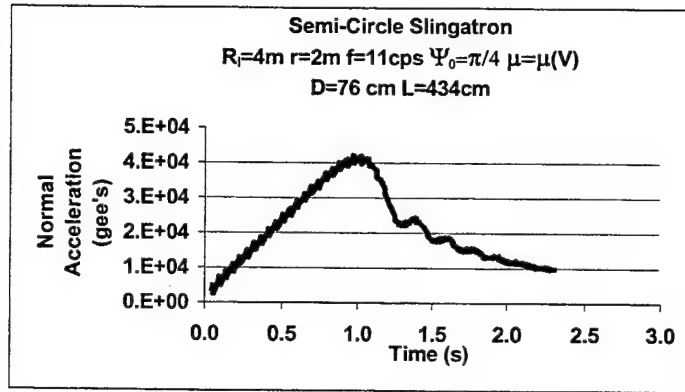


Fig. 16 Normal component of acceleration vs. time for the semi-circle slingatron

In a similar fashion the parallel component of acceleration, $A_{//} = -\ddot{s}$, is plotted in Fig. 17 where for comparison we also plot $|F_{\perp}|/M$.

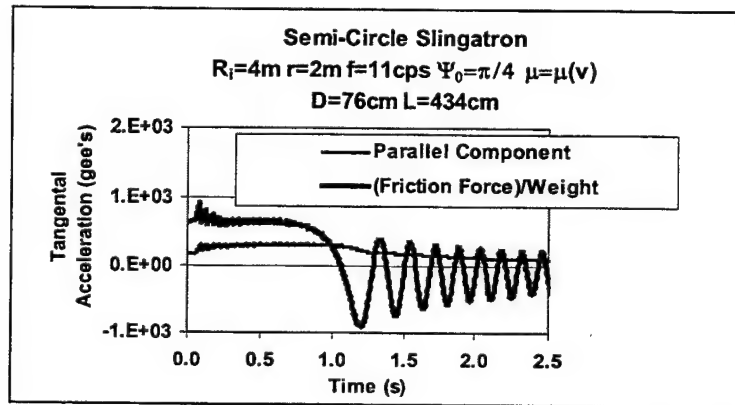


Fig. 17 Comparison of parallel component of acceleration and friction force/weight vs. time

Comparing Fig. 16 with Fig. 17 verifies that the time t where the maximum velocity is found is also the time where friction force per unit mass equals $A_{//}$, thus substantiating the conclusion mentioned above.

Examining the curvature of the semi-circle slingatron shows that R'' is not continuous at the points, $\phi = n\pi$, $n = 0, 1, 2, \dots$, where the upper half plane semi-circles

meet the lower half plane semi-circles, see Eqn. (15-16). However, these discontinuities of the sleds acceleration are not severe enough to cause numerical integration problems of Eq. (4).

Further Illustrations

Before leaving the topic of spiral shaped slingatrons we will give results for two other familiar spiral shaped tracks. Both of these configurations have the non-zero initial velocity, $\phi(0) = 0$ and $\dot{\phi}(0) = 2\pi f$. The first is the parabolic spiral given by

$$R(\phi) = R_i + r \sin(\psi_0) \phi^2. \quad (20)$$

A velocity plot for this is given in Fig. 18

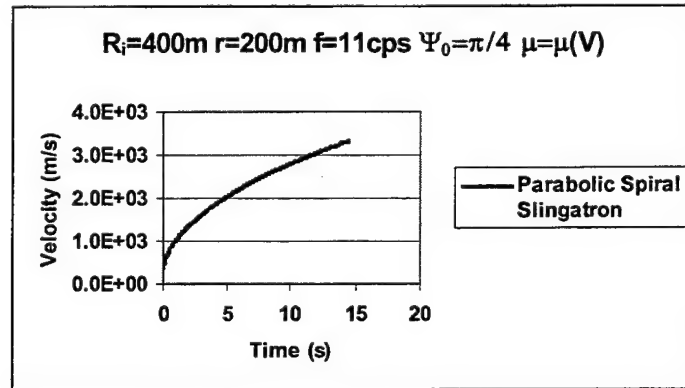


Fig. 18 Velocity vs. time for the parabolic spiral slingatron

for which the friction coefficient μ is modeled using Eq. (17). The last case considered is the logarithmic spiral given by

$$R(\phi) = R_i + r \sin(\psi_0) \ln(\phi). \quad (21)$$

The velocity for this spiral is presented in Fig. 19 where again the coefficient μ is calculated using Eq. (17).

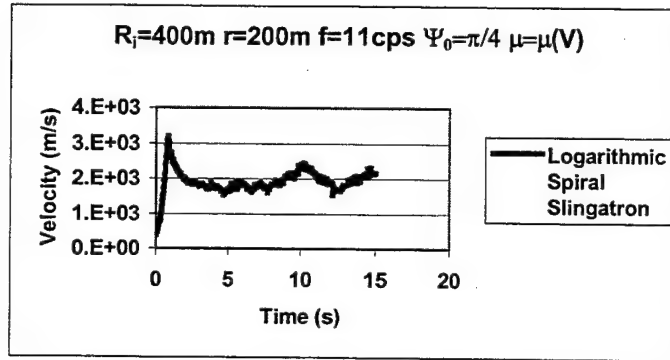


Fig. 19 Velocity vs. time for the parabolic spiral slingatron

One can see from the last two plots that a wide variety of choices for, $R(\phi)$, r , ψ and f , are possible to obtain large maximum sled velocities. These choices offer considerable flexibility when faced with design constraints for a spiral shaped slingatron.

Conclusion

The closed loop circular slingatrons require the gyration arm, r , to accelerate, $\ddot{\psi} > 0$, in order for the mass sled to reach substantial maximum velocities. As time progresses the sled is optimally accelerated as indicated by the lock-in angles θ approaching nearly a constant value. Experience from generating computer simulations, for the closed circular slingatron, reveal that initial sled velocities close to $\dot{\phi}(0) = 2\pi f$ are necessary in order to gain substantial sled acceleration.

The spiral slingatrons are able to produce sufficiently large maximum sled velocities using only constant angular gyration speeds, $\ddot{\psi} = 0$. All of the small-scale spiral slingatrons require initial injection velocities in the neighborhood of $\dot{\phi}(0) = 2\pi f$ in order to gain large maximum speeds. However, the large-scale version of the semi-circle slingatron has an additional favorable feature in that it can generate large maximum

velocities with zero initial injection sled velocities. This will make such slingatrons mechanically easier to build. Examination of the bearing pressure and the corresponding magnitude of the sled acceleration give insight into the stress levels that the sled and spiral track must endure.

The empirical friction model shows that the maximum velocity is very sensitive to $\mu(\hat{V})$. Furthermore, we found unlimited sled velocities for a proper choice of the parameter ψ_0 . There are a variety of choices regarding the spiral shape, $R(\phi)$, as well as the parameters r, ψ, ψ_0 and f that one can make in order to produce a large range of maximum sled velocities. Even though the results given here strongly suggest that spiral shaped tracks are the most desirable, the optimal spiral configuration is still an unanswered question. Experiments and further modeling to address the high velocity dependence of $\mu(\hat{V})$ are slated to take place in the near future.

References

- ¹Tidman, D. A. "Sling Launch of a Mass Using Superconducting Levitation", IEEE Transactions on Magnetics, Vol. 32, No.1, 1996, pp 240-247
- ²Tidman, D. A. "Slingatron Mass Launchers", Journal of Propulsion and Power, Vol. 14, No. 4, pp. 537-544, July-August, 1998. See also Tidman D. A., US Patents 5,699,779, Dec. 1997: 5,950,608, Sept. 14, 1999; and 6,014,964, Jan. 18,2000.
- ³Tidman, D. A. "private communication" and notes."

<u>NO. OF COPIES</u>	<u>ORGANIZATION</u>	<u>NO. OF COPIES</u>	<u>ORGANIZATION</u>
2	DEFENSE TECHNICAL INFORMATION CENTER DTIC OCA 8725 JOHN J KINGMAN RD STE 0944 FT BELVOIR VA 22060-6218	1	DIRECTOR US ARMY RESEARCH LAB AMSRL CI AI R 2800 POWDER MILL RD ADELPHI MD 20783-1197
1	HQDA DAMO FDT 400 ARMY PENTAGON WASHINGTON DC 20310-0460	3	DIRECTOR US ARMY RESEARCH LAB AMSRL CI LL 2800 POWDER MILL RD ADELPHI MD 20783-1197
1	OSD OUSD(A&T)/ODDR&E(R) DR R J TREW 3800 DEFENSE PENTAGON WASHINGTON DC 20301-3800	3	DIRECTOR US ARMY RESEARCH LAB AMSRL CI IS T 2800 POWDER MILL RD ADELPHI MD 20783-1197
1	COMMANDING GENERAL US ARMY MATERIEL CMD AMCRDA TF 5001 EISENHOWER AVE ALEXANDRIA VA 22333-0001		<u>ABERDEEN PROVING GROUND</u>
1	INST FOR ADVNCD TCHNLGY THE UNIV OF TEXAS AT AUSTIN 3925 W BRAKER LN STE 400 AUSTIN TX 78759-5316	2	DIR USARL AMSRL CI LP (BLDG 305)
1	DARPA SPECIAL PROJECTS OFFICE J CARLINI 3701 N FAIRFAX DR ARLINGTON VA 22203-1714		
1	US MILITARY ACADEMY MATH SCI CTR EXCELLENCE MADN MATH MAJ HUBER THAYER HALL WEST POINT NY 10996-1786		
1	DIRECTOR US ARMY RESEARCH LAB AMSRL D DR D SMITH 2800 POWDER MILL RD ADELPHI MD 20783-1197		

INTENTIONALLY LEFT BLANK.

REPORT DOCUMENTATION PAGE			Form Approved OMB No. 0704-0188	
<small>Public reporting burden for this collection of information is estimated to average 1 hour per response, including the time for reviewing instructions, searching existing data sources, gathering and maintaining the data needed, and completing and reviewing the collection of information. Send comments regarding this burden estimate or any other aspect of this collection of information, including suggestions for reducing this burden, to Washington Headquarters Services, Directorate for Information Operations and Reports, 1215 Jefferson Davis Highway, Suite 1204, Arlington, VA 22202-4302, and to the Office of Management and Budget, Paperwork Reduction Project(0704-0188), Washington, DC 20503.</small>				
1. AGENCY USE ONLY (Leave blank)		2. REPORT DATE September 2001		3. REPORT TYPE AND DATES COVERED Reprint, July 2000–December 2000
4. TITLE AND SUBTITLE Numerical Simulations of the Slingatron			5. FUNDING NUMBERS 1L162618.AH80	
6. AUTHOR(S) Gene R. Cooper, Derek A. Tidman,* Mark L. Bundy, and Stephen Wilkerson				
7. PERFORMING ORGANIZATION NAME(S) AND ADDRESS(ES) U.S. Army Research Laboratory ATTN: AMSRL-WM-BC Aberdeen Proving Ground, Maryland 21005-5066			8. PERFORMING ORGANIZATION REPORT NUMBER ARL-RP-30	
9. SPONSORING/MONITORING AGENCY NAMES(S) AND ADDRESS(ES) NASA Goddard Space Flight Center Greenbelt Road East Greenbelt, MD 20770			10. SPONSORING/MONITORING AGENCY REPORT NUMBER	
11. SUPPLEMENTARY NOTES * ALCorp., 6801 Benjamin Street, McLean, VA 22101 A reprint from Proceedings of the 10th U.S. Army Gun Dynamics Symposium, Austin, TX, 23-26 April 2001.				
12a. DISTRIBUTION/AVAILABILITY STATEMENT Approved for public release; distribution is unlimited.			12b. DISTRIBUTION CODE	
13. ABSTRACT (Maximum 200 words) The slingatron mass accelerator is described for several track configurations (shapes), and numerical simulations of this accelerating mass traversing a given track configuration are presented. The sled is modeled as a point mass that interacts with the slingatron track using both a conventional and a new empirical velocity dependent friction law. The closed loop circular slingatron was found to produce high maximum sled velocities provided the gyration angular speed is always increasing. In contrast several spiral shaped slingatron tracks reveal that high maximum sled velocities are obtainable with the gyration speed held constant. In fact, a slingatron constructed out of semi-circles is shown capable of generating high velocity sleds in such a way that no initial sled injection is necessary. Choosing the proper initial gyration phase with an empirically determined friction model allows the mass sled to gain ever-increasing velocities when placed in a semi-circle slingatron. The sled bearing pressure and its total acceleration are examined and presented.				
14. SUBJECT TERMS slingatron, sled, spiral, circle, numerical			15. NUMBER OF PAGES 27	
			16. PRICE CODE	
17. SECURITY CLASSIFICATION OF REPORT UNCLASSIFIED	18. SECURITY CLASSIFICATION OF THIS PAGE UNCLASSIFIED	19. SECURITY CLASSIFICATION OF ABSTRACT UNCLASSIFIED	20. LIMITATION OF ABSTRACT UL	

INTENTIONALLY LEFT BLANK.